A Numerical Study of a non-Newtonian Flow Problem

by

M.F. Webster†
ICFD, Department of Mathematics,
University of Reading, U.K.

E.E. Suli and K.W. Morton
Oxford University Computing Laboratory;
Numerical Analysis Group,
University of Oxford, U.K.

Numerical Analysis Report 8/86

Key Words: Steady incompressible non-Newtonian flow
Forward-facing step Second-order model Linear
Nonlinear Elliptic Hyperbolic Convergence
Stability Iteration Marching Finite differences
Stream function Vorticity Stress

This work forms part of the research programme of the Institute for Computational Fluid Dynamics at the Universities of Oxford and Reading.

†Present address: Department of Mathematics and Computer Science, University College of Swansea, Singleton Park, Swansea SA2 8PP,U.K.

A Numerical Study of a non-Newtonian Flow Problem

by

M.F.Webster
ICFD,Department of Mathematics,University of Reading,UK.†

E.E.Suli and K.W.Morton
Oxford University Computing Laboratory;Numerical Analysis Group,
University of Oxford,UK.

Numerical Analysis Report 8/86

Key Words: Steady incompressible non-Newtonian flow
Forward-facing step Second-order model Linear Nonlinear
Elliptic Hyperbolic Convergence Stability Iteration
Marching Finite differences Stream function Vorticity
Stress

This work forms part of the research programme of the Institute for Computational Fluid Dynamics at the Universities of Oxford and Reading.

†Present address: Department of Mathematics and Computer Science,
University College of Swansea,Singleton Park,Swansea SA2 8PP,UK.

CONTENTS

Summary

A finite difference strategy is presented to solve equations of the Navier-Stokes type when coupled with a stress equation. Steady planar two-dimensional flows of an incompressible non-Newtonian fluid are considered. The variables chosen to describe the flow are stream function, stress and vorticity. The system of nonlinear differential equations involved is linearised introducing a Picard-type iteration. The discretised linear equations that result are solved by a combination of secondary iterations and marching. The convergence of the iteration and the stability of the difference scheme are analysed for the forward-facing step problem. Particular attention is paid to the dependence of the Picard iteration upon the relevant material parameters. Results are presented for the second-order non-Newtonian fluid model.

1 Introduction

1.1 Scope of paper

In this paper, we consider a simple model problem which typifies the numerical difficulties that arise in non-Newtonian flow analysis. We propose a numerical scheme which solves equations of a Navier-Stokes type when coupled with a stress equation. The flow is steady, planar, two-dimensional and incompressible and the flow variables adopted are stream function ψ and vorticity ω.

The model problem corresponds to the so-called second-order fluid model(SOE). The SOE exhibits a constant viscosity μ and its extra-stress components have an explicit dependence upon the velocity field. This model has the attraction that the vorticity equation may be expressed solely in terms of the velocity and the vorticity. Our analysis takes particular advantage of this feature to investigate the numerical effects that arise. The SOE is, however, only physically realistic for slow flows or for slightly elastic fluids.

The equation system to be solved may be stated in the following non-dimensional form:

$$W\underline{u}.\underline{\nabla}(\nabla^2\omega) + R\underline{u}.\underline{\nabla}\omega - \nabla^2\omega = 0 \ , \tag{1a}$$

$$\nabla^2\psi + \omega = 0 \ , \tag{1b}$$

$$\underline{u} = \underline{\nabla} \times \psi\hat{\underline{k}} = \left[\frac{\partial\psi}{\partial y}, -\frac{\partial\psi}{\partial x}\right] \ . \tag{1c}$$

The two non-dimensional parameters that appear are the Reynolds number R and the Weissenberg number W (an elasticity parameter) defined as

$$R = \frac{\rho UL}{\mu} \quad \text{and} \quad W = \frac{\lambda U}{L} \ , \tag{2}$$

where U is a characteristic (mean) velocity, L is a characteristic length, ρ is the fluid density, μ is the dynamic fluid viscosity, and λ is a relaxation time: characteristic values are selected from a fully-developed downstream flow station.

The techniques developed here are applicable in a general flow situation that may be described by a coupled system of the incompressible flow equations and a stress equation system. This naturally leads to the consideration of more realistic non-Newtonian stress models(cf.Walters[1]), buoyancy driven flows and some models for turbulent flows.

The present approach introduces a further auxiliary "stress-like" variable ζ. This scalar variable (henceforth referred to as the stress) is defined through the identity

$$\zeta = \nabla^2\omega \ . \tag{3}$$

The full system of equations (1) and (3) is then considered in a form with (1a) replaced by

$$W\underline{u}.\underline{\nabla}\zeta - \zeta = -R\underline{u}.\underline{\nabla}\omega \ , \tag{4}$$

representing two elliptic equations and a hyperbolic equation.

This system of equations is discretised by finite difference methods on a uniform grid: the usual five-point operator is used for (1b) and (3), with (4) replaced by a Crank-Nicolson scheme. The resulting system of nonlinear algebraic equations is solved iteratively by successive substitutions. This introduces a sequence of Picard-type iterations at the nonlinear (outer) level. The order of computation within one such iteration is to first compute ζ, then ω and finally ψ, from which the next velocity field iterate is evaluated. At the linear equation (inner) level a combination of inner iterations for the

elliptic equations and direct marching for the hyperbolic equation is used.

The convergence of the outer iteration and the stability of the marching scheme are analysed for the forward-facing step problem over a range of values of the two-parameter family (R,W). We are particularly interested in covering the full range of W values for R≤O(10).

1.2 Historical background

This paper concentrates on a traditional iterative approach: decoupling by linearisation, reducing the nonlinear equation system into a set of linear equations and introducing an outer Picard iteration. The present iterative scheme is compared to two similar iteration schemes proposed by Crochet and Pilate[2] and Davies[3]. Using a non-negative outer iteration number n these schemes may be summarised as follows:

$$W\underline{u}^n.\underline{\nabla}(\nabla^2\omega^q) + R\underline{u}^n.\underline{\nabla}\omega^r - \nabla^2\omega^s = 0 \ , \tag{5a}$$

$$\nabla^2\psi^{n+1} + \omega^{n+1} = 0 \ , \tag{5b}$$

$$\underline{u}^{n+1} = \underline{\nabla} \times \psi\underline{\hat{k}}^{n+1} \ , \tag{5c}$$

where for Scheme 1(Crochet) q=r=s=n+1; for Scheme 2(Davies) q=n, s=n+1, R≡0; and for Scheme 3(Present) q=s=n+1, r=n.

Scheme 1 yields a third-order differential equation for ω leading to convergence difficulties in the corresponding inner iteration. Solutions were reported for the (R,W) values of {(1,0.1),(10,0.2), (100,0.4),(500,0.8),(1000,1.4)}. A critical upper limit on W was observed for each selected R value, though this limit increased with increase in R. This phenomenon of a restrictive upper limit on W is common throughout non-Newtonian computational flow analysis and

remains a crucial issue to resolve. The present study addresses this problem and provides insight into the nature of this phenomenon. Scheme 2, with R≡0, gives an efficient inner ω iteration but W is effectively limited by the numerical smoothing of the source term $W\underline{u}^n.\underline{\nabla}(\nabla^2\omega^n)$. Solutions were reported for (R,W) of {(0,0.1), without filtering; (0,W),W≤10 with filtering}. The present scheme differs from Schemes 1 and 2 by the inclusion of a three-step outer iteration, and a direct marching scheme for $\nabla^2\omega$ at the linear level. No upper limit on W is found for converged solutions with R≤10, though Scheme 3 exhibits a restriction on R.

The acceptibility of converged solutions for small R values is based on the Tanner/Geisekus theorem(see, for example,[4]) for creeping flow i.e.R≡0. At W=0 the solution for ζ is trivial, $\zeta = \nabla^2\omega = 0$, so that by Tanner's theorem the velocity field $\{\underline{u}\}_{W=0}$ also satisfies the problem for all W>0.

2 Analysis of outer iterations

In order to obtain some feel for the dependence of the outer iteration on the parameters R and W, a linearised perturbation analysis using a single Fourier mode is considered. We introduce the following notation:

$$\omega = \Omega + \hat{\omega}\exp(\iota\underline{\kappa}.\underline{x}) \ , \tag{6a}$$

$$\psi = \Psi + \hat{\psi}\exp(\iota\underline{\kappa}.\underline{x}) \ , \tag{6b}$$

$$\underline{u} = \underline{U} + \hat{\underline{u}}\exp(\iota\underline{\kappa}.\underline{x}) \ , \tag{6c}$$

where $\iota=\sqrt{-1}$ and Ω, Ψ and $\underline{U}$ satisfy the original differential problem

$$\underline{U}.\underline{\nabla}(R\Omega + W\nabla^2\Omega) - \nabla^2\Omega = 0 \ , \tag{7a}$$

$$\nabla^2\Psi + \Omega = 0 \ , \tag{7b}$$

$$\underline{U} = \underline{\nabla} \times \Psi\hat{\underline{k}} \ . \tag{7c}$$

For Scheme 1 the outer iteration for the linearised equations yields

$$\iota(\underline{U}.\underline{\kappa})(R - \kappa^2 W)\hat{\omega}^{n+1} + \kappa^2\hat{\omega}^{n+1} = -\underline{G}.\hat{\underline{u}}^n \quad , \tag{8}$$

where

$$\underline{G}.\hat{\underline{u}}^n = \iota(\underline{G} \times \underline{\kappa})\hat{\psi}^n = \iota\kappa^{-2}(\underline{G} \times \underline{\kappa})\hat{\omega}^n \quad , \tag{9}$$

and $\underline{G} = \underline{\nabla}(R\Omega + W\nabla^2\Omega)$. Thus convergence of the iteration requires

$$\frac{|\underline{G} \times \underline{\kappa}|}{\kappa^2\,|\kappa^2 + \iota(\underline{U}.\underline{\kappa})(R - \kappa^2 W)|} < 1 \quad . \tag{10}$$

Clearly, for a given flow and specified $\underline{U}$, $\underline{G}$, R and W, it is the lowest frequencies(i.e.longest wavelengths $|\underline{\kappa}|$) which will give most trouble. Also in a reasonably narrow channel the longest wavelength modes that can occur in the system are likely to be roughly along the streamlines so that $\underline{U}.\underline{\kappa}_{min} \neq 0$. Thus for a fixed Reynolds number R, as W is increased from zero, not only the numerator in (10) increases but also the denominator attains a minimum when $W \approx R/\kappa^2_{min}$. Thus a limit on W might be expected for which convergence can be achieved, and that this will increase with R.

Similarly, the outer iteration for the linearised equations in Scheme 3 gives

$$\kappa^2\left[1 - \iota W(\underline{U}.\underline{\kappa})\right]\hat{\omega}^{n+1} = -\underline{G}.\hat{\underline{u}}^n - \iota R(\underline{U}.\underline{\kappa})\hat{\omega}^n \tag{11}$$

which for convergence requires

$$\frac{|\underline{G} \times \underline{\kappa} + R\kappa^2(\underline{U}.\underline{\kappa})|}{\kappa^4\,|1 - \iota W(\underline{U}.\underline{\kappa})|} < 1 \quad . \tag{12}$$

In this case, increasing W increases the denominator, provided $\underline{U}.\underline{\kappa} \neq 0$, and an extra term in R appears in the numerator. Clearly, the left hand side of (12) is smaller than that of (10) unless $R\kappa^2(\underline{U}.\underline{\kappa})$ dominates $\underline{G} \times \underline{\kappa}$ or R dominates $\kappa^2 W$. In particular, if $|\underline{G} \times \underline{\kappa}| < \kappa^4$ so that (10) is satisfied, then (12) is also satisfied if

$R\kappa^2 |\underline{U}.\underline{\kappa}| + |\underline{G} \times \underline{\kappa}| < \kappa^4$. Hence Scheme 3 will exhibit a less severe restriction on W for small R but this situation will deteriorate more rapidly with increasing R.

In contrast to the above, Scheme 2 leads to

$$\kappa^2 \hat{\omega}^{n+1} = -\underline{G}.\hat{\underline{u}}^n + \iota W\kappa^2 (\underline{U}.\underline{\kappa})\hat{\omega}^n \qquad (13)$$

where $\underline{G} = W\underline{\nabla}(\nabla^2\Omega)$ and again convergence requires

$$W|\underline{\kappa} \times \underline{\nabla}(\nabla^2\Omega) + \kappa^4(\underline{U}.\underline{\kappa})| < \kappa^4 \ . \qquad (14)$$

Here both high and low frequencies give trouble - hence the need for filtering. The bound on $|\underline{\kappa}|$ due to high frequencies is roughly proportional to W^{-1} (see Tanner[5]) so that again it is increasing W that leads to non-convergence.

For a rigorous convergence analysis of the iteration between ω and ψ we refer to Smith[6,7], Ehrlich[8] and McLaurin[9]. The need for introducing such an iteration arises partly because ω is unspecified on the rigid boundaries. References[6,7,8,9] study the coupled equation approach to solving the biharmonic equation for ψ in a rectangular domain. The biharmonic boundary value problem is reduced to a coupled system of Poisson equations, which depend on an arbitrary coupling parameter c. This system may be solved by iteration. Maclaurin proved that the iteration converges for all sufficiently small values of c: namely if $0<c<2\nu_1$, where ν_1 is the smallest eigenvalue of the corresponding Dirichlet eigenvalue problem[9]. In the finite difference approximations of the coupled system the coupling constant is no longer arbitrary. Indeed, $c=2h^{-1}$, where h is the step size. Unfortunately, this iteration is divergent unless averaging is used, as shown by Smith[6]. Given one of the averaging parameters, there is an optimal choice of the other(cf.Ehrlich[8] and McLaurin[9]). Although this analysis is only valid for Stokesian flow in a rectangular region with rigid

boundaries, it provides us with some indication about the appropriate choices of the averaging parameters in our iteration procedure.

3 Full statement of the model problem

We consider the forward-facing step problem for the model equations discussed earlier and written in the following form:

$$W\underline{u}^n . \underline{\nabla}\zeta^{n+1} - \zeta^{n+1} = -R\underline{u}^n . \underline{\nabla}\omega^n \ , \tag{15a}$$

$$\nabla^2\omega^{n+1} = \zeta^{n+1} \ , \tag{15b}$$

$$\nabla^2\psi^{n+1} = -\omega^{n+1} \ , \tag{15c}$$

$$\underline{u}^{n+1} = \underline{\nabla} \times \psi\hat{\underline{k}}^{n+1} \ , \tag{15d}$$

where $\underline{u} = (u,v)$. The region of solution is shown in Fig.1: ABCD is a rigid boundary, FE is a symmetry boundary, AF is the inlet boundary and DE is the outlet boundary. The flow is assumed to be fully-developed at inlet and outlet. Denoting the outward normal to the boundary by N, the appropriate boundary conditions are as follows:

Rigid boundary ABCD

$$u = v = 0 \qquad \Rightarrow \quad \psi = 0, \ \omega = \pm\partial^2\psi/\partial N^2, \ \zeta = 0 \ ; \tag{16a}$$

Inflow boundary AF

$$u \text{ given}, \ v = \frac{\partial v}{\partial x} = 0 \quad \Rightarrow \quad \psi, \ \omega \text{ given} \ ; \tag{16b}$$

Outflow boundary DE

$$v = 0, \ \frac{\partial\omega}{\partial x} = \frac{\partial\zeta}{\partial x} = 0 \quad \Rightarrow \quad \frac{\partial\psi}{\partial x} = \frac{\partial\omega}{\partial x} = 0, \ \zeta = 0 \ ; \tag{16c}$$

Symmetry boundary EF

$$\frac{\partial u}{\partial y} = 0, \ v = 0 \qquad \Rightarrow \quad \psi = \psi_F, \ \omega = \zeta = 0 \ . \tag{16d}$$

Since DE and AF are effectively assumed to be at $x=\pm\infty$ there is a superfluity of boundary conditions available at inflow and outflow. The conditions actually used are given in (16) after the "implies" symbol: the minimum assumptions required appear before the symbol. The

boundary conditions for ζ are particularly significant and will be referred to again below. As a result of these choices, AB and CD can be reasonably small for accurate results to be achieved. The inlet velocity profile does, however, incorporate a further assumption that $\partial^2\omega/\partial y^2=0$. The non-dimensionalised form of (15) yields the inlet conditions

$$\psi = 0.5b(3a^2 - 4y^2)y + \psi_F,\ u = 1.5b(a^2 - 4y^2),\ \omega = 12by, \quad (17)$$

with $a=4$, $b=a^{-3}$, $\psi_F=-0.5$ and a flow rate of 1/2 unit over the 1/2 unit channel width DE. Apart from R and W the only other parameter in the problem is the contraction ratio AF:DE which is taken to be 4:1.

The objective is to compute flows for a range of values of R and W in the domain of Fig.1. For R=W=0 the flow is Stokesian. For W=0 the equations reduce to the Navier-Stokes equations (combining (15a) with (15b) and ignoring the boundary conditions for ζ) and again the flow is well documented(cf.Dennis and Smith[10]). In particular, for $R\geq 0$ a recirculating region develops in the corner ABC. This is a weak vortex which initially decreases in size and strenght as R is increased up to $R\approx 50$. After $R\approx 50$ this primary eddy increases monotonically with R giving rise to secondary eddies and, eventually, the flow becomes turbulent for $2000\leq R\leq 3000$. Additionally, above $R\approx 500$ a second separation region is anticipated to occur beyond C on CD[11,12]. The present study is confined to the range $0\leq R\leq 10$.

When W>0 the flow patterns that arise at fixed R vary greatly with the physical properties of the non-Newtonian fluid. For example, for $R\leq O(10)$ as W increases from zero, some elastic fluids with a reasonably constant viscosity (e.g.Boger fluids[13]) show no significant vortex behaviour beyond that exhibited by the equivalent Newtonian fluid[14]. Alternatively, certain elastic fluids with a shear-thinning

viscosity can render a substantial corner vortex[15,16]. Here we focus our attention on a constant viscosity fluid described by the SOE model.

Introducing a small positive value of W leads to the consideration of a singular perturbation problem. In general, a boundary layer for ζ is expected, depending on the boundary conditions imposed for the solution of (15a). The symmetry boundary condition $\zeta=0$ holds as $W \to 0$ as does that on the fixed boundary: thus the only difficulty that may occur is at inflow or outflow. The condition $\zeta=0$ is imposed at outflow because, considered as an ordinary differential equation along the streamlines, (15a) has an exponentially decreasing complementary solution in the upstream direction. If CD is reasonably large (so that there is no forcing term in (15a) near DE), no boundary layer difficulties arise. In particular, for R=0 it follows that ζ is identically zero for any value of W as it should be.

There remains the problem of the singularity at C and the calculation of ζ in the recirculating flow region when $R \neq 0$. These issues are discussed in the next section.

4 Numerical approximation

4.1 Finite difference equations

The region Ω of Fig.1 is covered by a regular square grid of step size h and nodal values of the variables ψ, ω, ζ at x=ih, y=jh are denoted by $\psi_{i,j}$ etc. Values of h of 1/8 and 1/16 are used, requiring some 1400 mesh points and 16 mesh lengths at inflow for the former choice. The following standard notation is used for the difference operators:

$$\delta_x \psi_{i+1/2,j} = \psi_{i+1,j} - \psi_{i,j} \quad ,$$
$$\mu_x \psi_{i+1/2,j} = (\psi_{i+1,j} + \psi_{i,j})/2 \quad , \tag{18}$$

with similar meaning for δ_y and μ_y. The difference approximations to the Poisson equations for ω and ψ are then the standard five-point schemes:

$$(\delta_x^2 + \delta_y^2)\omega_{i,j}^{n+1} = h^2 \zeta_{i,j}^{n+1} \quad ,$$
$$(\delta_x^2 + \delta_y^2)\psi_{i,j}^{n+1} = -h^2 \omega_{i,j}^{n+1} \quad , \tag{19}$$

Here the superscript n+1 denotes the stage of the outer iteration process, $\zeta^{n+1} \rightarrow \omega^{n+1} \rightarrow \psi^{n+1}$.

Two different schemes are used for the stress equation: the box scheme in the recirculating flow region Ω_h^1 and the Crank-Nicolson type scheme in Ω_h^2 where the flow is predominantly in the x-direction. For the former, velocities are required at each cell-centre (i+1/2,j+1/2) and are given by the four-point formulae

$$u_{i+1/2,j+1/2}^n = h^{-1} \mu_x \delta_y \psi_{i+1/2,j+1/2}^n \quad ,$$
$$v_{i+1/2,j+1/2}^n = -h^{-1} \mu_y \delta_x \psi_{i+1/2,j+1/2}^n \quad . \tag{20a}$$

Then the box scheme approximation to (15a) is

$$W\left[(u^n \mu_y \delta_x + v^n \mu_x \delta_y)\zeta^{n+1}\right]_{i+1/2,j+1/2}$$
$$- h\left[\theta \mu_x \mu_y \zeta_{i+1/2,j+1/2} + (1-\theta)\zeta_{i,j+1}\right]^{n+1}$$
$$= -R\left[(u^n \mu_y \delta_x + v^n \mu_x \delta_y)\omega^n\right]_{i+1/2,j+1/2} \tag{20b}$$

where the parameter θ permits pointwise weighting and ensures stability for all possible velocity fields. The Crank-Nicolson scheme covers two neighbouring cells with the same x-coordinate and is

therefore centred at (i+1/2,j). Thus the velocities are given by the unsymmetric formulae

$$u^n_{i+1/2,j} = h^{-1}\mu_x\mu_y\delta_y\psi^n_{i+1/2,j} \ ,$$
$$v^n_{i+1/2,j} = -h^{-1}\delta_x\psi^n_{i+1/2,j} \ , \tag{21a}$$

and the approximation to (15a) is

$$\left[W(u^n\delta_x + v^n\mu_x\mu_y\delta_y)\zeta^{n+1} - h\hat{\zeta}^{n+1}\right]_{i+1/2,j}$$
$$= -R\left[(u^n\delta_x + v^n\mu_x\mu_y\delta_y)\omega^n\right]_{i+1/2,j} \tag{21b}$$

where

$$\hat{\zeta}_{i+1/2,j} = \beta\zeta_{i+1,j} + (1-\beta)\zeta_{i,j} \ . \tag{21c}$$

The weighting parameter β is introduced to ensure the stability of the scheme and its choice will be discussed later.

Let us focus our attention on the treatment of the boundary conditions for these schemes. For ψ^n in (19), Dirichlet conditions are supplied from (16a,b,d) for all boundaries but DE. From (16c), the Neumann condition for both ψ^n and ω^n on DE is satisfied through

$$\psi^n_{I,j} = \psi^n_{I-1,j} \ , \quad \omega^n_{I,j} = \omega^n_{I-1,j} \ . \tag{22}$$

Dirichlet conditions are imposed on ω^n on AF and EF from (16b,d). It remains to specify ω^n on the wall ABCD. This is achieved by a Taylor series expansion of the local wall velocity conditions. With reference to Fig.2, we use the following derived formulae:

$$\omega^n_{i,J} = -2h^{-2}(\psi_{i,J-1} - \psi_{i,J})^{n-1} \ , \tag{23a}$$

$$\omega^n_{i,J} = -3h^{-2}(\psi_{i,J-1} - \psi_{i,J})^{n-1} - 1/2\omega^r_{i,J-1} \ , \tag{23b}$$

$$\omega^n_{I,J} = -2h^{-2}(\psi_{I-1,J} + \psi_{I,J-1} - 2\psi_{I,J})^{n-1} \ , \tag{23c}$$

where I and J are wall coordinates, (I,J) is the re-entrant corner C, and r in (23b) may be chosen as outer iteration level n-1 or n. Formula (23a) is formally first-order accurate(see Thom[17]);formula (23b) is second-order accurate(see Woods[18]), and is used with r=n at all wall points bar C; formula (23c) is attributed to Kawaguti[19] and provides a finite estimate of ω_C^n based on (23a). It is well known that for the Navier-Stokes equations ω is unbounded at C (cf.Moffatt[20]): however, formula (23c) generates an estimate closely approximating that provided by the finite difference strategy of Holstein and Paddon[21] which matches an asymptotic expansion in the corner neighbourhood.

For stability reasons the equations for ζ^{n+1} are integrated from outflow to inflow, and from (16a,c,d) ζ^{n+1} is set to zero on all boundaries except at inflow AF. The fully-developed flow conditions at inflow provide a compatability check on the numerical solution and, for consistency, ζ^{n+1} should decay in the entry region and vanish at the inflow boundary. Thus if the Crank-Nicolson scheme were to be used over the whole region Ω_h sufficient data would now be available, with $\{\psi,\omega\}^n_{i,j}$ specified at all interior and boundary points: the same is true if the box scheme (20) is incorporated in a limited zone Ω_h^1 based on ABC but not extending across to the symmetry boundary EF.

4.2 **Solution procedure**

At the beginning of the stage n → n+1, a set of $\psi^n_{i,j}$ will be known from which the streamlines can be drawn and the extent of the recirculating region defined(i.e.where $\psi^n>0$). ζ^{n+1} is then calculated as follows. First, the box scheme (20) is introduced for the recirculation zone Ω_h^1 proceeding in a point-wise manner. Commencing

at the cell in the corner B, ζ^{n+1} at the corner diagonally opposite to B is calculated provided ψ^n at that point is within Ω_h^1: this is continued for cells along BC until the corresponding ψ^n falls outside Ω_h^1. This process is repeated for the next j-column of cells moving out into the flow, and hence covering the whole of the recirculating region. The resulting values of ζ^{n+1} then constitute a lower boundary condition for sweeping the Crank-Nicolson scheme (21) from outflow to inflow in the non-recirculating region Ω_h^2. It is vital to restrict the application of the box scheme to Ω_h^1 alone. Otherwise large numerical oscillations in ζ^{n+1} may occur cross-stream which will subsequently be swept upstream by the marching scheme. This is due to the sign switch that occurs in the box scheme when v^n dominates u^n. The weighting factor θ in the box scheme varies between 0 and 1 pointwise. Its choice guarantees the stability of the scheme for all possible variations in the velocity field.

Second, the Crank-Nicolson scheme is used in Ω_h^2 which involves a direct line-by-line marching procedure in the upstream direction. At each value i=I+1,I,... a tridiagonal system emerges which relates $(\zeta_{j+1},\zeta_j,\zeta_{j-1})_I^{n+1}$ to $(\zeta_{j+1},\zeta_j,\zeta_{j-1})_{I+1}^{n+1}$, for cross-stream j-values, through

$$\left[V\zeta_{j+1} - (U+h(1-\beta))\zeta_j - V\zeta_{j-1}\right]_I^{n+1} + \left[V\zeta_{j+1} + (U-\beta h)\zeta_j - V\zeta_{j-1}\right]_{I+1}^{n+1} = f_{I+1/2,j}^n \qquad (24)$$

where $V = 0.25Wv_{I+1/2,j}^n$ and $U = Wu_{I+1/2,j}^n$. A fast tridiagonal solver is used to solve the system of equations (24). The Crank-Nicolson scheme is only applicable for the region Ω_h^2 where the flow is predominantly in the streamwise direction. If it is extended to cover

Ω_h^1 a large cross-stream oscillation in ζ^{n+1} is observed due to relatively small local velocity field values there; this then leads to a failure to converge in the Picard iteration.

Next the Poisson equations (19) for ω^{n+1} followed by that for ψ^{n+1}, are solved by secondary inner iterations: SOR is used for this purpose, but clearly other methods may also be applicable. We have utilised the empirically estimated optimal relaxation factors of $1.6 \leq \varrho_\psi \leq 1.8$ and $\varrho_\omega = 1.0$(see Davies et al.[22]).

The smoothing factors on the outer iterates are $\chi_\psi = 0.1$ and $\chi_\omega = \chi_\zeta = 0.3$ where, for example,

$$\psi^{n+1} = \chi_\psi \psi^n + (1-\chi_\psi)\hat{\psi}^{n+1} \tag{25}$$

and $\hat{\psi}^{n+1}$ represents the current unsmoothed iterate. These choices are consistent with the work of others[6,7,8,9] discussed in Section 2. Additionally, in order to guarantee the stability of the outer iteration, we restrict ourselves to a single ω iteration per outer iteration cycle. Utilising graded iterative convergence tolerances with less stringent restrictions on ω than ψ produces a similar effect (see Webster[23]). The essential nature of such practices becomes apparent when the residuals of the equations are monitored as the Picard iteration proceeds.

4.3 Stability of the marching scheme

First, the tridiagonal matrix for each I-line is considered. Clearly, the associated matrix for (24) will be diagonally dominant for an upstream march direction provided

$$|U + h(1-\beta)| \geq 2|V| \tag{26}$$

for j-values spanning the cross-stream section of Ω_h^2. Within Ω_h^2, $u^n_{I+1/2,j}$ remains non-negative and is expected to dominate $v^n_{I+1/2,j}$

almost everywhere. The inequality (26) will be satisfied with least restriction on the relevant velocity conditions when β vanishes. This then provides a sufficiency condition which guarantees the numerical stability of the tridiagonal matrix solver(cf.Golub and van Loan[24]). Furthermore, from a 1-D analysis for a simple channel flow, the condition $\beta \leq U/h$ must be satisfied to avoid streamwise oscillations on the grid scale when implementating the Crank-Nicolson scheme.

Next, the sensitivity to perturbations of the marching sweep is Fourier analysed, in a manner akin to an iteration process in decreasing I-values. Consider the perturbation $\delta\zeta_{I+1,j}$ on $\zeta_{I+1,j}$ which gives rise to the corresponding perturbation of $\delta\zeta_{I,j}$ on $\zeta_{I,j}$. These perturbations satisfy (24) and may be expressed as

$$\delta\zeta_{I,j} = \sum_m \lambda_m^I \exp(\iota j \xi_m) \ , \ \iota = \sqrt{-1} \ , \tag{27}$$

with Fourier coefficients λ_m^I where m is the mode number. Substitution of (27) into (24) gives for the m-th component,

$$\lambda_m^I \left[(U+h-\beta h) - \iota 2V\sin\xi_m \right] = \lambda_m^{I+1} \left[(U-\beta h) + \iota 2V\sin\xi_m \right] . \tag{28}$$

The Fourier stability criterion for a stable marching sweep in the upstream direction is the amplification factor condition $|\lambda_m^I/\lambda_m^{I+1}| \leq 1$ for all modes m. This criterion is satisfied if

$$(U - \beta h)^2 \leq (U + h - \beta h)^2 \tag{29}$$

for all cross-stream j-values in Ω_h^2: that is if $\beta \leq 0.5 + U/h$. Clearly for the choice $\beta=0$ stability is affirmed and oscillations on the grid scale are avoided provided $u^n_{I+1/2,j} \geq 0$ over the region in question. Hence the necessity to restrict the marching scheme to flow zones where the flow is predominantly in the streamwise direction.

5 Results

Relative tolerances in $[\zeta, \omega, \psi]$ of $[10^{-2}, 10^{-2}, 10^{-3}]$ are used to monitor the convergence of the iteration procedure. It is generally observed that, as R is increased, the convergence criteria become increasingly more difficult to satisfy. The convergence of the Picard iteration is directly related to R: for small R convergence may be obtained for any W, whilst for larger R (greater than 10) convergence of the Picard iteration deteriorates for larger W. These findings are in agreement with the arguments of Section 2.

A selection of results is presented in Figs.3 - 6. For creeping flow (R=0) ζ vanishes for all $W \geq 0$. For $R=10^{-4}$ solutions are found for $10^{-4} \leq W \leq 10^{2}$: ζ behaves like $R\underline{u}.\underline{\nabla}\omega$ for $W \leq U^{-1}$ and like $\omega R/W$ for $W > U^{-1}$, where U is a characteristic velocity value. The same relative behaviour for ζ is observed for $R \leq 1$. The solutions for ζ for $0.1 \leq W \leq 10^{2}$ at R=1 and R=10 are shown for comparison in Figs.3 and 4. For completeness the solutions for ψ and ω are also given at W=1 for R=1 and R=10 in Fig.5. The diminished size of the vortex for ψ, between R=1 and R=10 for the comparable value of W=1, characterises the behaviour of ψ over a wide range of W at fixed R values: solutions for ψ and ω do not change significantly with W, only with R. Hence no vortex enhancement is observed for $R \leq 10$, in agreement with experimental results for some constant viscosity fluids that also manifest memory effects[14,16].

Fig.6 illustrates the tensor stress components P^{1k} (cf.Crochet et al.[25]) for the SOE model in the flow situations investigated. These components have a functional dependence upon derivatives of $\underline{u}$ up to the second order, whilst ζ depends on derivatives up to the third

order. In Fig.6 the first normal-stress difference $P^{xx} - P^{yy}$ and the shear stress P^{xy} are displayed at R=1 for W=1 and W=10, where normalisation is performed with respect to the corresponding downstream fully-developed wall value.

6 Conclusions

A finite difference scheme has been developed to study incompressible flows of various types: a non-Newtonian fluid is considered here. The new features involved are the direct marching scheme for the stress equation and the particular choice of the outer iteration scheme. The study of this and similar iteration schemes has led to a broader understanding of their behaviour with respect to the material parameters involved. Indeed, for the second-order model the convergence of the present scheme is directly related to R, and for $R \leq O(10)$ solutions may be obtained for a wide range of W. Hence, for this benchmark problem proceeding in the manner prescribed, no restrictive upper limit on W is encountered for $R \leq 10$.

These techiques can be applied to Maxwell/Oldroyd models(cf.Oldroyd[26]) and a Newton-type iteration scheme may then be appropriate. Furthermore, the multi-grid method may be used in either a nonlinear or a linear fashion, to account for the sensitivity of the iteration schemes to long wavelength error modes. These issues will be studied elsewhere.

References

1. K.Walters, Rheometry,Chapman & Hall,London,1975.

2. M.J.Crochet and G.Pilate,'Plane flow of a fluid of second grade through a contraction',J. Non-Newtonian Fluid Mech.,1,247-258 (1976).

3. A.R.Davies,'Numerical filtering and the high Weissenberg number problem',J. Non-Newtonian Fluid Mech.,16,195-209(1984).

4. R.I.Tanner,'Plane creeping flows of incompressible second-order fluids',Phys. Fluids,9(I),1246-1247(1966).

5. R.I.Tanner,'The stability of some numerical schemes for model viscoelastic fluids',J. Non-Newtonian Fluid Mech.,10,169-174 (1982).

6. J.Smith,'The coupled equation approach to the numerical solution of the biharmonic equation by finite differences (I)',SIAM J. Numer. Anal.,5(2),323-339(1968).

7. J.Smith,'The coupled equation approach to the numerical solution of the biharmonic equation by finite differences (II)',SIAM J. Numer. Anal.,7(1),104-111(1970).

8. L.W.Ehrlich,'Solving the biharmonic equation as coupled finite difference equations',SIAM J. Numer. Anal.,8(2),278-287(1971).

9. J.W.McLaurin,'A general coupled equation approach for solving the biharmonic boundary value problem',SIAM J. Numer. Anal.,11(1), 14-33(1974).

10. S.C.R.Dennis and F.T.Smith,'Steady flow through a channel with a symmetrical constriction in the form of a step',Proc. R. Soc. Lond.,A372,393-414(1980).

11. S.Hickmott and R.M.Smith,CEGB UK Report No.TPRD/B/PS/292/M83 (1983).

12. F.Durst and T.Loy,'Investigations of laminar flow in a pipe with sudden contraction of cross sectional area',Comput. Fluids,13(1), 15-36(1985).

13. D.V.Boger,'A highly elastic constant-viscosity fluid', J. Non-Newtonian Fluid Mech.,3,87-91(1977/8).

14. K.Walters and D.M.Rawlinson,'On some contraction flows for Boger fluids',Rheol. Acta,21,547-552(1982).

15. J.L.White and A.Kondo,'Flow patterns in polyethylene and polystyrene melts during extrusion through a die entry region: measurement and interpretation',J. Non-Newtonian Fluid Mech.,3, 41-64(1977/8).

16. K.Walters and M.F.Webster,'On dominating elastico-viscous response in some complex flows',Phil. Trans. R. Soc. Lond.,A308, 199-218(1982).

17. A.Thom,'The flow past circular cylinders at low speeds',Proc. R. Soc. Lond.,A141,651-666(1933).

18. L.C.Woods,'A note on the numerical solution of fourth order differential equations',Aeron. Q.,5(III),176(1954).

19. M.Kawaguti,Mathematical Research Centre Report No.574,University of Wisconsin, Madison(1965).

20. H.K.Moffatt,'Viscous and resistive eddies near a sharp corner', J. Fluid Mech.,18,1-18(1964).

21. H.Holstein and D.J.Paddon,'A finite difference strategy for re-entrant corner flow',In "Numerical Methods for Fluid Dynamics", Academic Press,London,(Eds. K.W.Morton and M.J.Baines),341-358 (1982).

22. A.R.Davies,K.Walters and M.F.Webster,'Long range memory effects in flows involving abrupt changes in geometry (III): moving boundaries',J. Non-Newtonian Fluid Mech.,4,325-344(1979).

23. M.F.Webster,Ph.D. thesis,University of Wales,Aberystwyth(1979).

24. G.H.Golub and C.F.van Loan, Matrix Computations,North Oxford Academic,Oxford,1983.

25. M.J.Crochet,A.R.Davies and K.Walters, Numerical simulation of non-Newtonian flow,Elsevier,New York and Amsterdam,1983.

26. J.G.Oldroyd,'On the formulation of rheological equations of state',Proc. R. Soc. Lond.,A200,523-541(1950).

Figure legend

Fig. 1. Schematic flow diagram.

Fig. 2. Mesh near boundary.

Fig. 3. Stress ζ contours.

R = 1; (a) W = 0.1, (b) W = 1, (c) W = 10, (d) W = 100.

Contour key.

Fig. 4. Stress ζ contours.

R = 10; (a) W = 0.1, (b) W = 1, (c) W = 10, (d) W = 100.

Contour key.

Fig. 5. Stream function and vorticity contours.

W = 1; (a) ψ , (b) ω , R = 1;

(c) ψ , (d) ω , R = 10.

Contour key.

Fig. 6. First normal-stress difference and shear stress.

R = 1; (a) $P^{xx} - P^{yy}$, (b) P^{xy} , W = 1;

(c) $P^{xx} - P^{yy}$, (d) P^{xy} , W = 10.

Contour key.

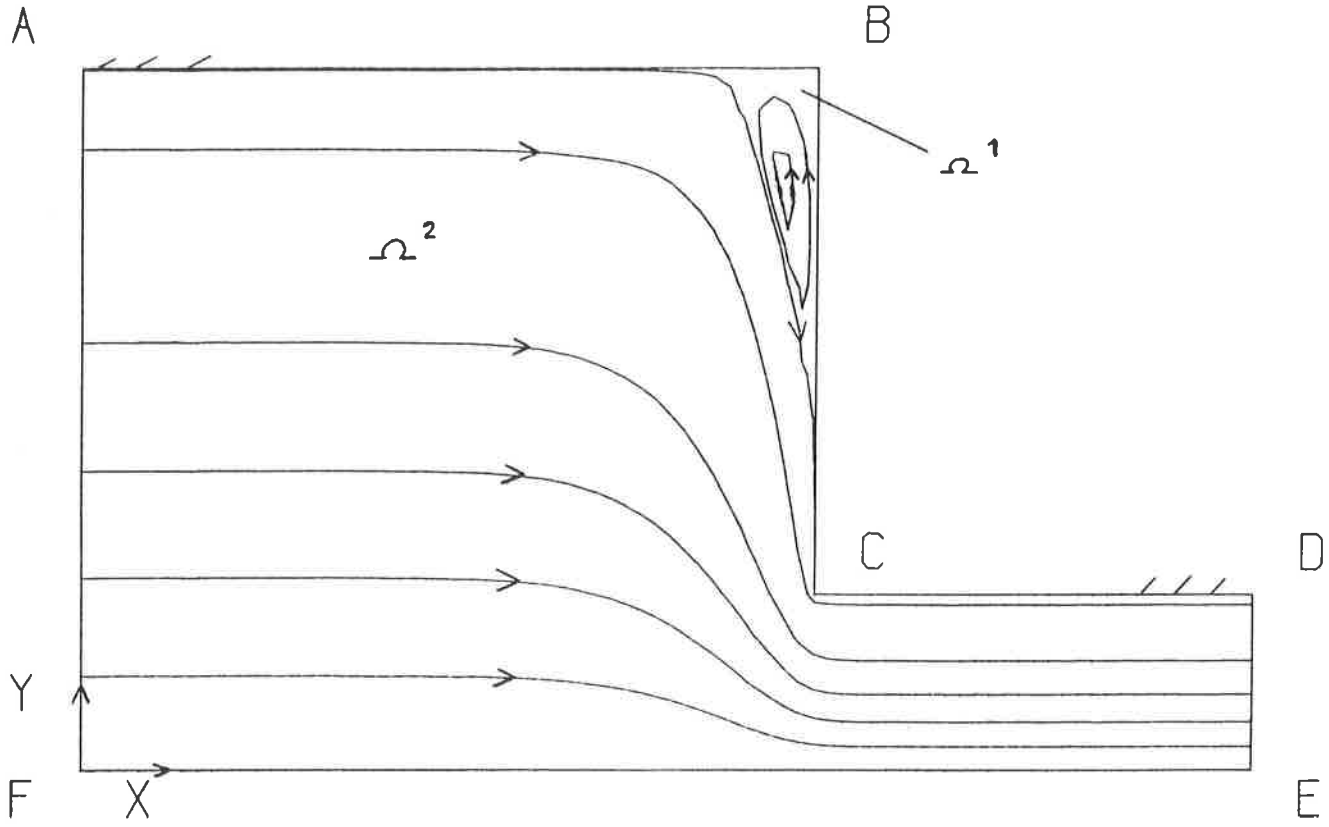

Fig. 1. Schematic flow diagram

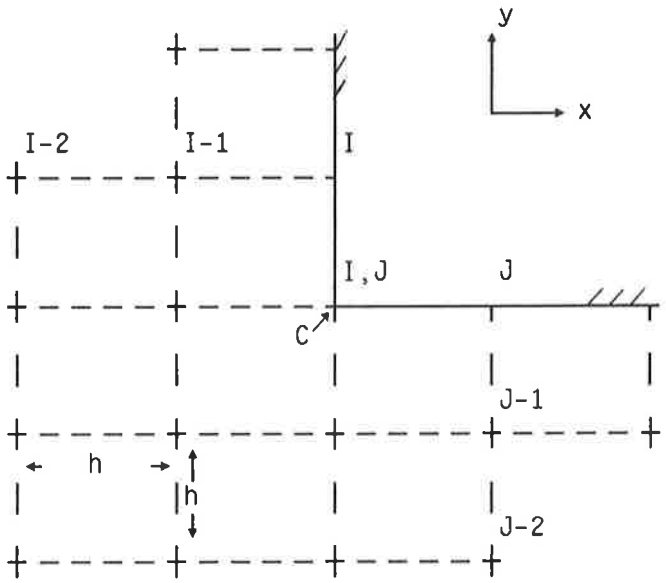

Fig. 2. Mesh near boundary

STRESS (a) R=1, W=.1

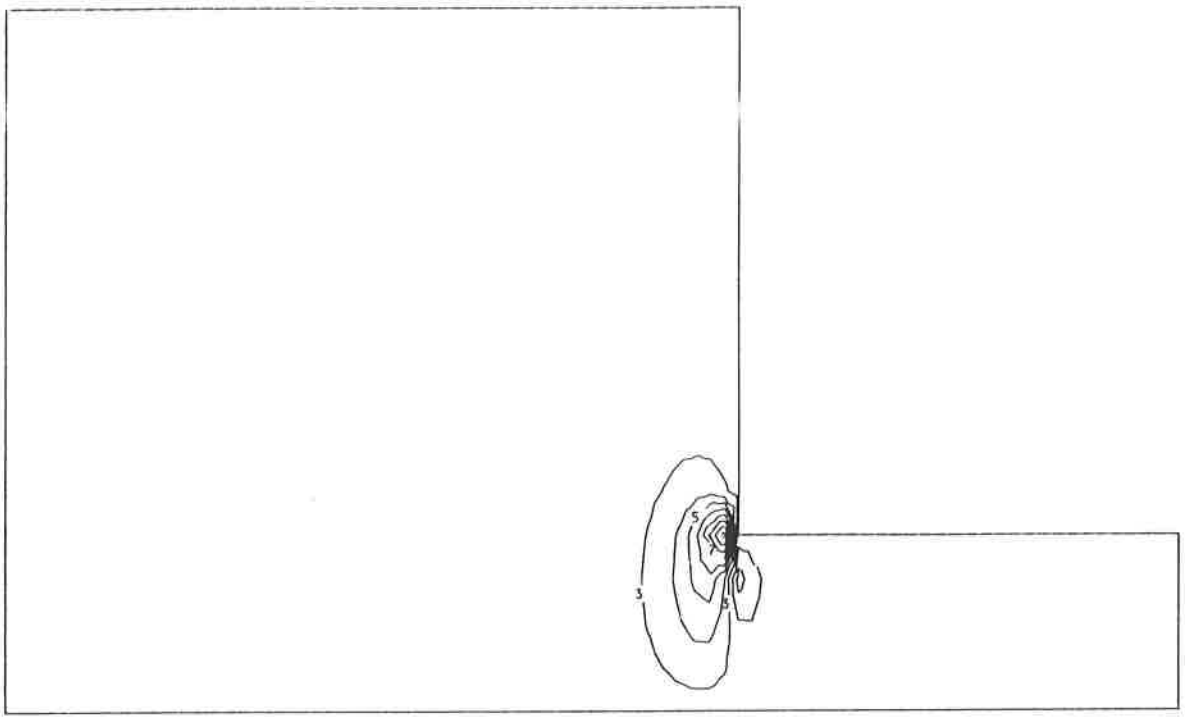

STRESS (b) R=1, W=1

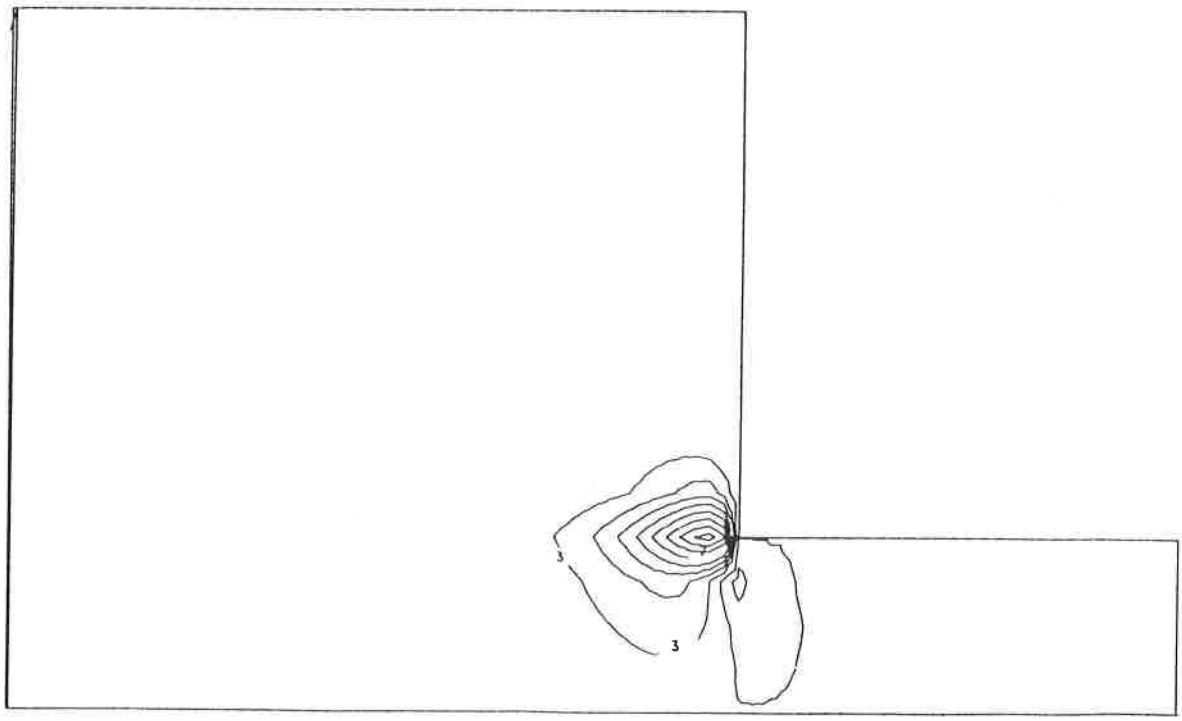

Fig. 3. (a) and (b)

(a) R=1, W=.1 CONTOUR KEY	
1	-2.29388
2	-0.78500
3	0.72388
4	2.23277
5	3.74165
6	5.25053
7	6.75941
8	8.26829
9	9.77717
10	11.28605

(b) R=1, W=1 CONTOUR KEY	
1	-0.62905
2	-0.01353
3	0.60200
4	1.21753
5	1.83305
6	2.44858
7	3.06411
8	3.67963
9	4.29516
10	4.91069

Fig. 3. (a) and (b)

STRESS (c) R=1, W=10

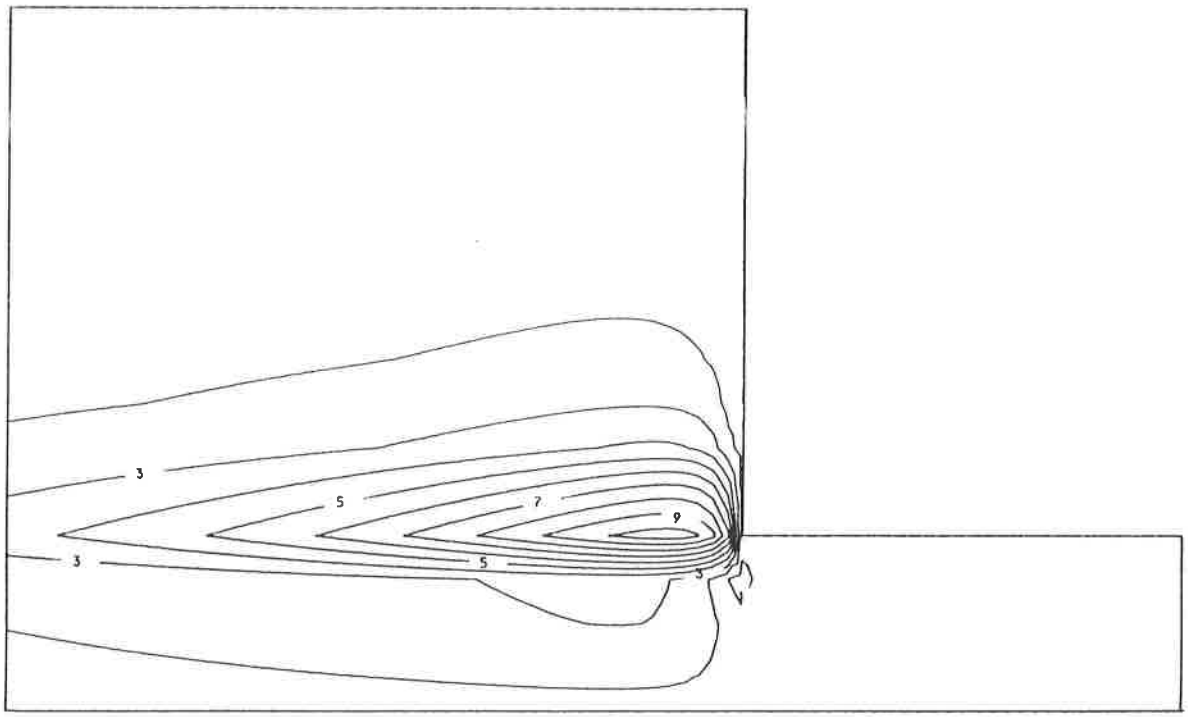

STRESS (d) R=1, W=100

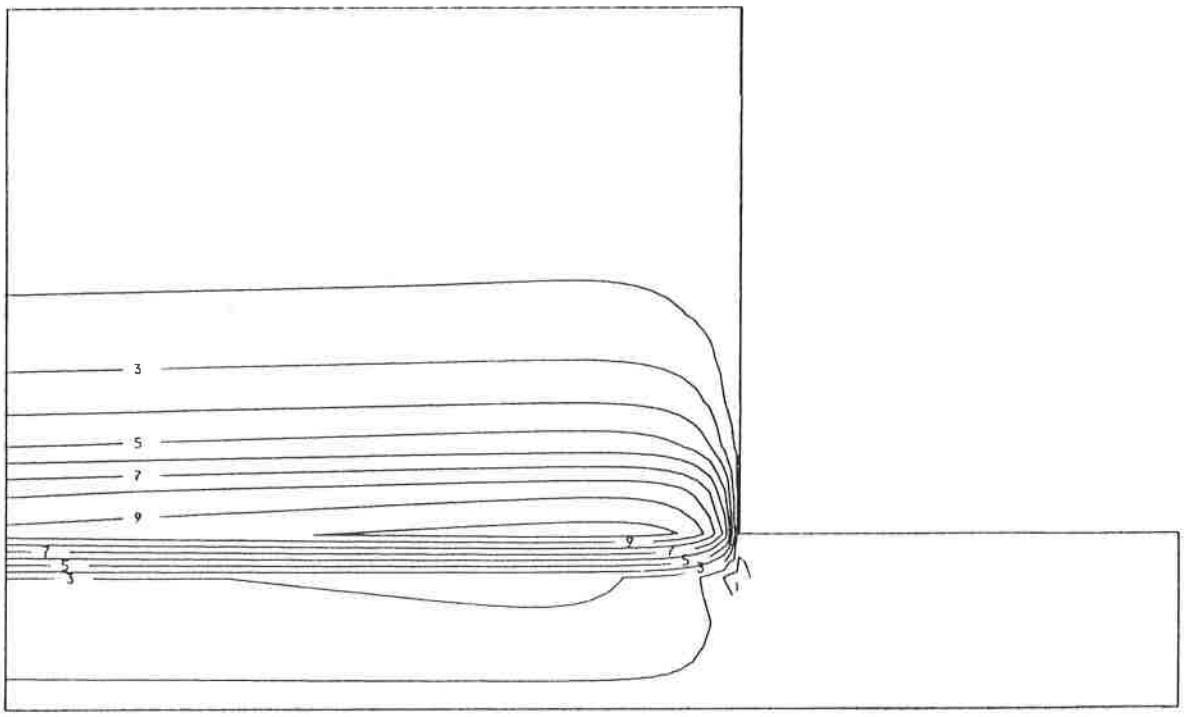

Fig. 3. (c) and (d)

(c) R=1, W=10

CONTOUR KEY	
1	-0.06571
2	0.03617
3	0.13804
4	0.23991
5	0.34179
6	0.44366
7	0.54554
8	0.64741
9	0.74928
10	0.85116

(d) R=1, W=100

CONTOUR KEY	
1	-0.00625
2	0.00512
3	0.01649
4	0.02786
5	0.03923
6	0.05060
7	0.06197
8	0.07334
9	0.08471
10	0.09608

Fig. 3. (c) and (d)

STRESS (a) R=10, W=.1

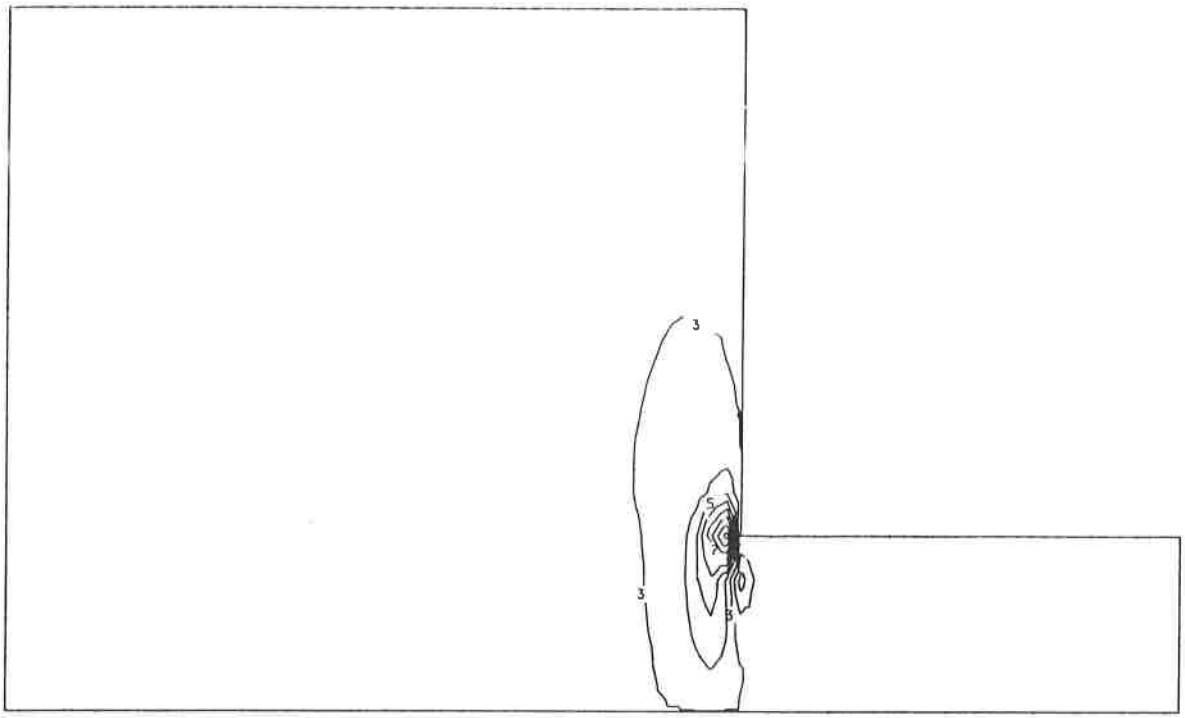

STRESS (b) R=10, W=1

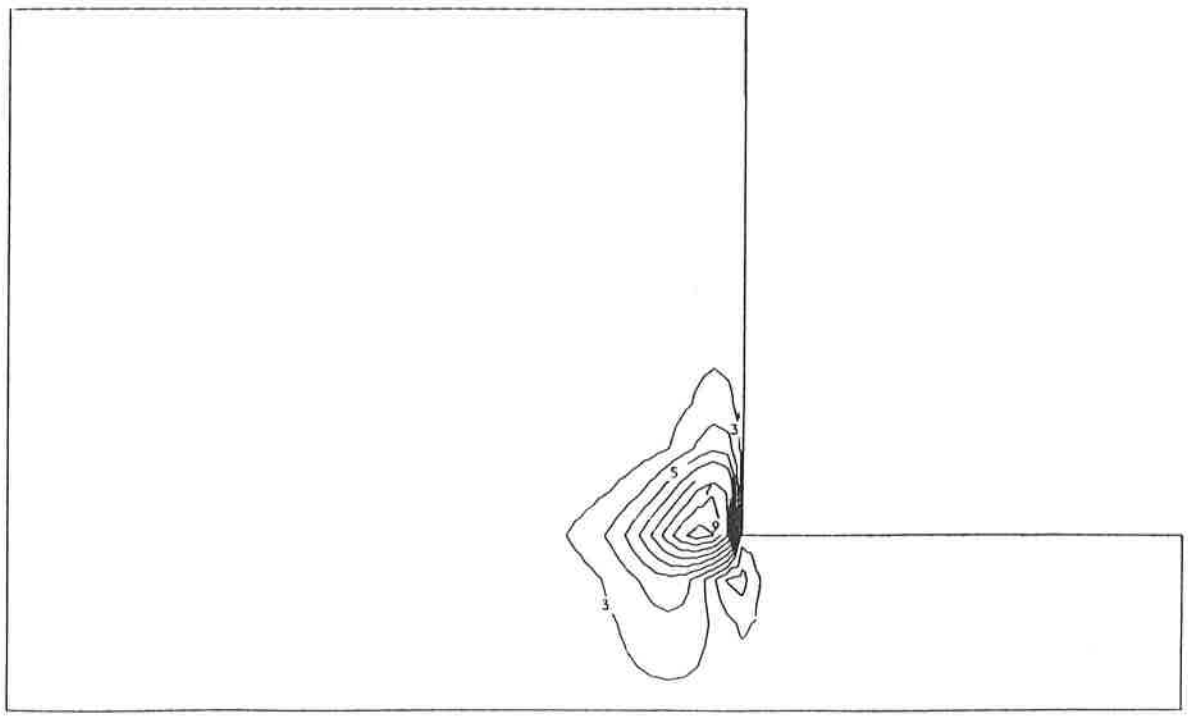

Fig. 4. (a) and (b)

(a) R=10, W=.1

CONTOUR KEY	
1	-51.45112
2	-25.37787
3	0.69537
4	26.76862
5	52.84187
6	78.91512
7	104.98837
8	131.06162
9	157.13487
10	183.20812

(b) R=10, W=1

CONTOUR KEY	
1	-13.88062
2	-4.62560
3	4.62941
4	13.88442
5	23.13943
6	32.39444
7	41.64946
8	50.90447
9	60.15948
10	69.41449

Fig. 4. (a) and (b)

STRESS (c) R=10, W=10

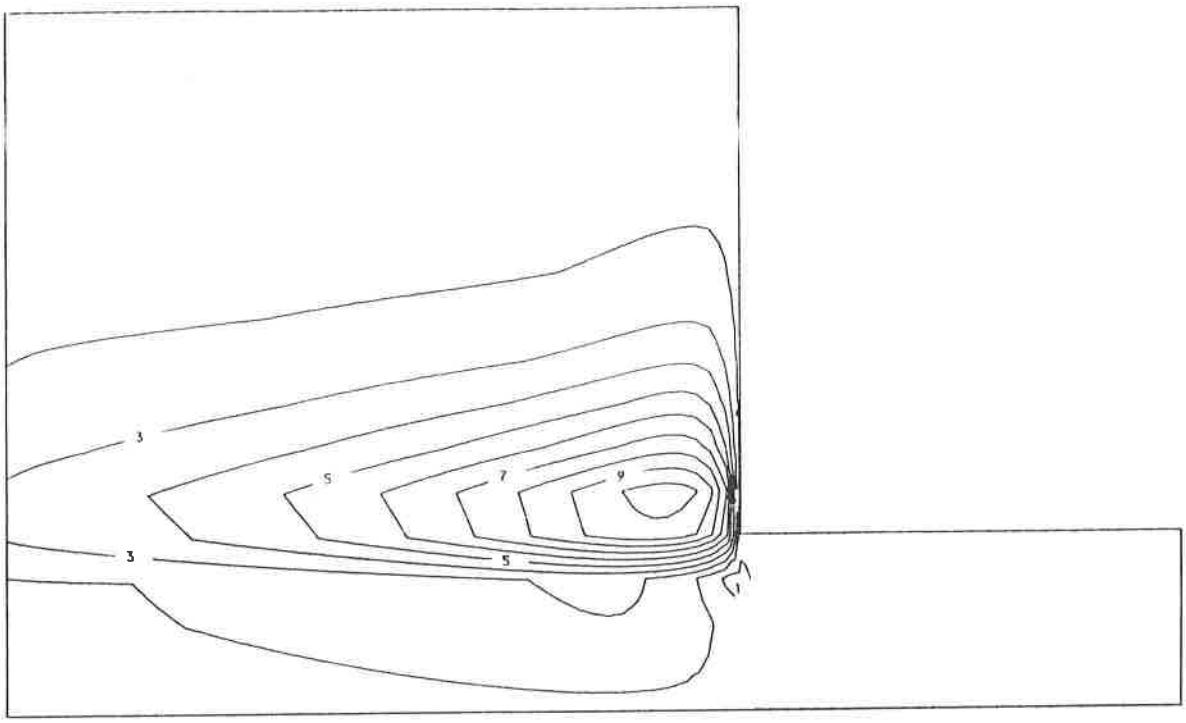

STRESS (d) R=10, W=100

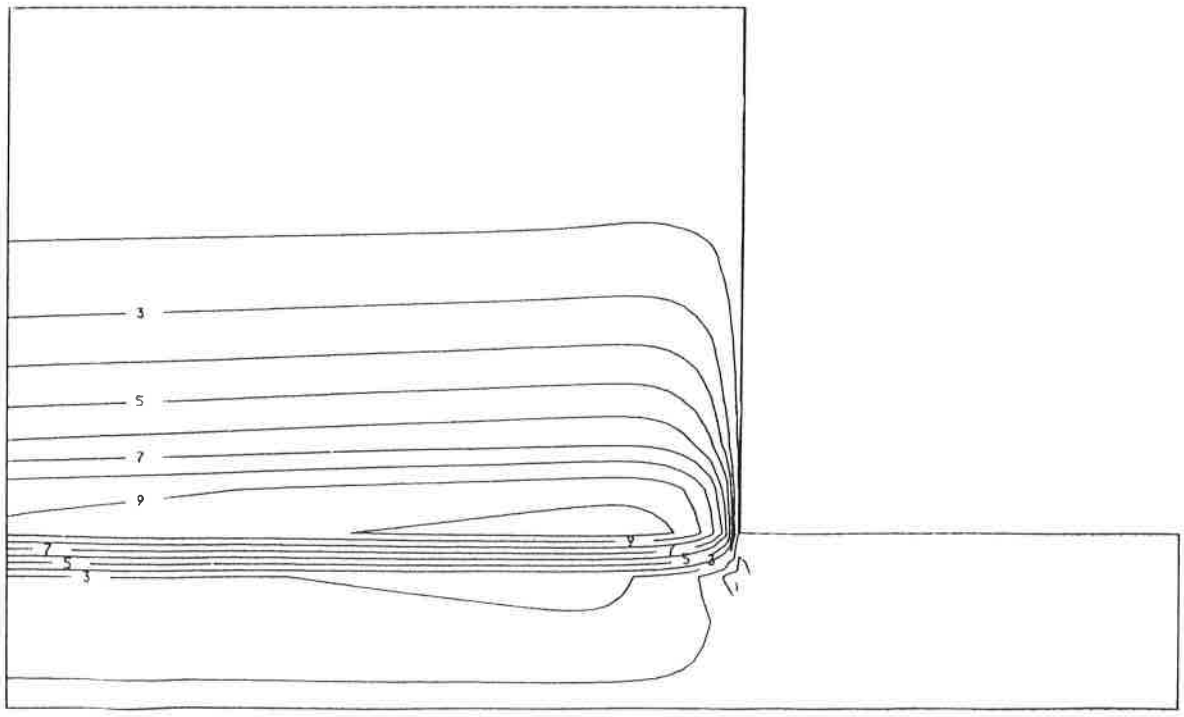

Fig. 4. (c) and (d)

(c) R=10, W=10

CONTOUR KEY	
1	-0.89063
2	0.31933
3	1.52929
4	2.73925
5	3.94921
6	5.15917
7	6.36913
8	7.57909
9	8.78905
10	9.99901

(d) R=10, W=100

CONTOUR KEY	
1	-0.06739
2	0.04809
3	0.16357
4	0.27906
5	0.39454
6	0.51003
7	0.62551
8	0.74100
9	0.85648
10	0.97196

Fig. 4. (c) and (d)

STREAMFUNCTION (a) R=1, W=1

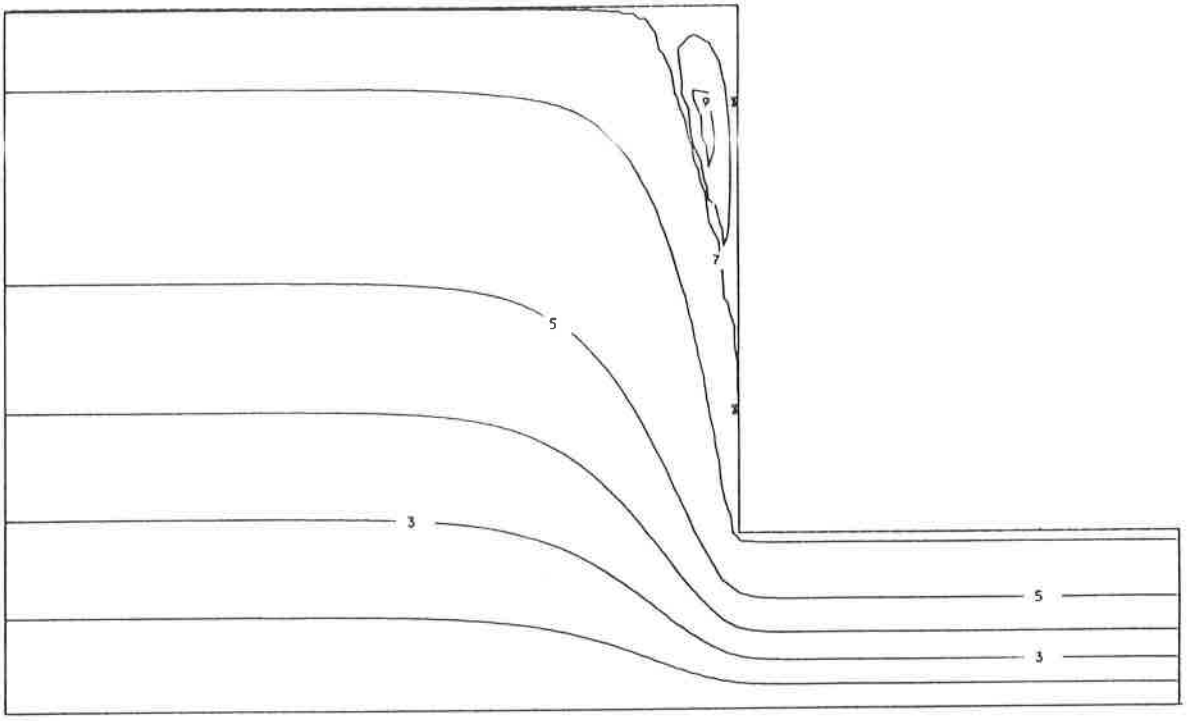

VORTICITY (b) R=1, W=1

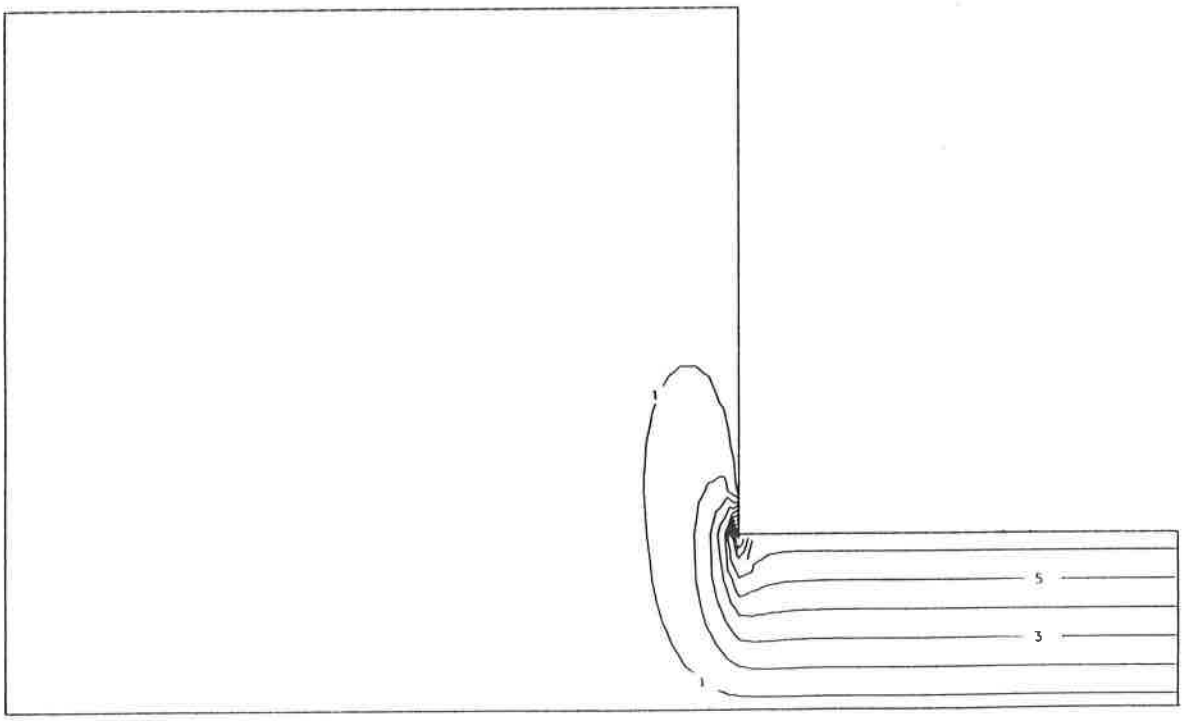

Fig. 5. (a) and (b)

(a) R=1.0 W= 1 CONTOUR KEY	
1	-0.50000
2	-0.40000
3	-0.30000
4	-0.20000
5	-0.10000
6	-0.01000
7	-0.00010
8	0.00010
9	0.00030
10	0.00050

(b) R=1.0 W=1 CONTOUR KEY	
1	0.44836
2	1.43818
3	2.42800
4	3.41782
5	4.40764
6	5.39746
7	6.38728
8	7.37710
9	8.36692
10	9.35674

Fig. 5. (a) and (b)

STREAMFUNCTION (c) R=10, W=1

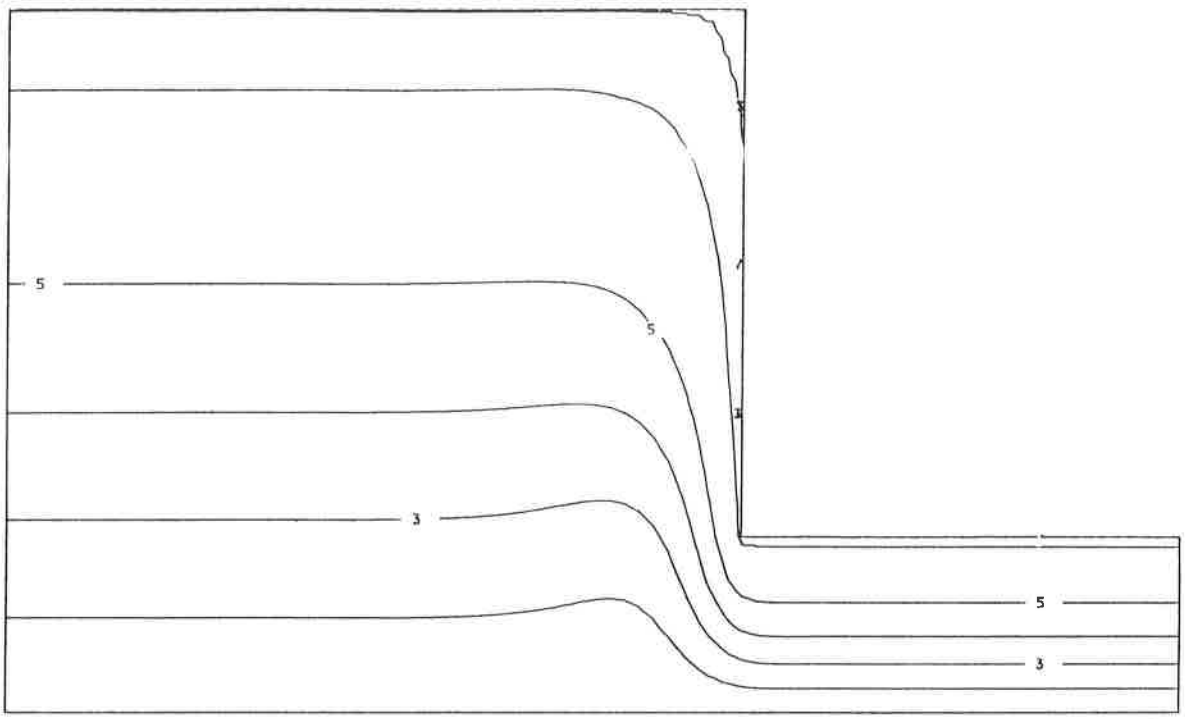

VORTICITY (d) R=10, W=1

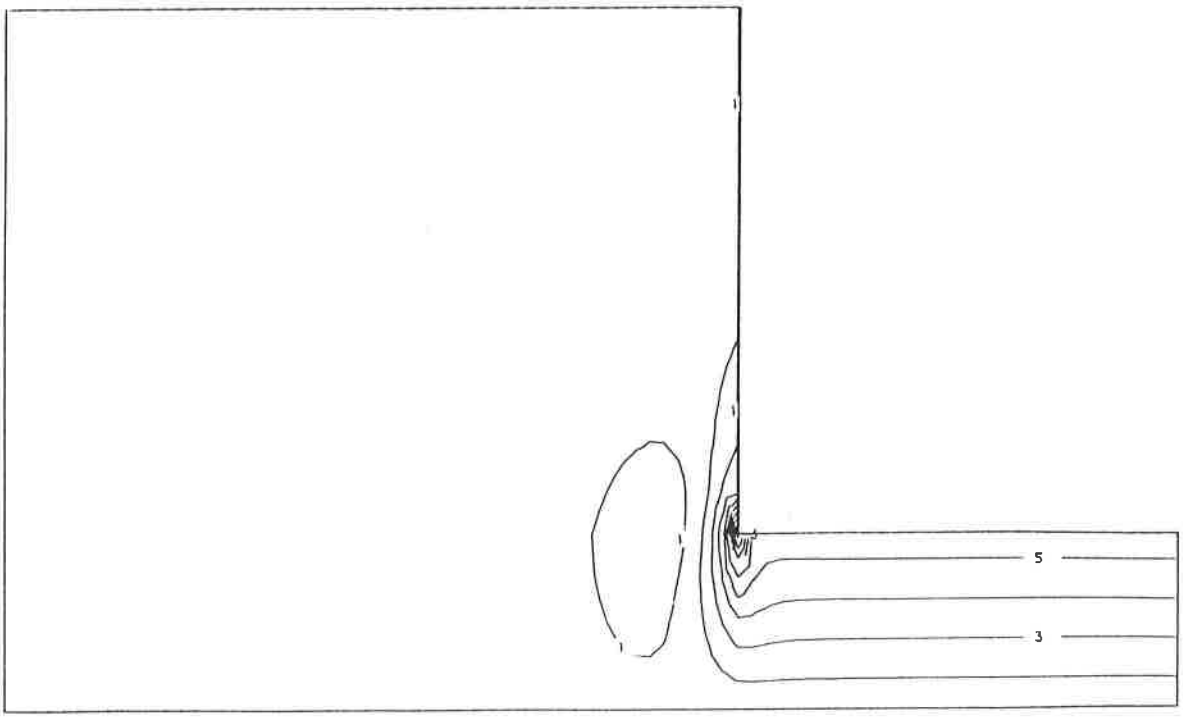

Fig. 5. (c) and (d)

(c) R=10, W=1

CONTOUR KEY

1	-0.50000
2	-0.40000
3	-0.30000
4	-0.20000
5	-0.10000
6	-0.01000
7	-0.00010
8	0.00010
9	0.00030
10	0.00050

(d) R=10, W=1

CONTOUR KEY

1	-0.33371
2	1.02682
3	2.38735
4	3.74788
5	5.10841
6	6.46894
7	7.82946
8	9.18999
9	10.55052
10	11.91105

Fig. 5. (c) and (d)

(a) PXX-PYY R=1, W=1

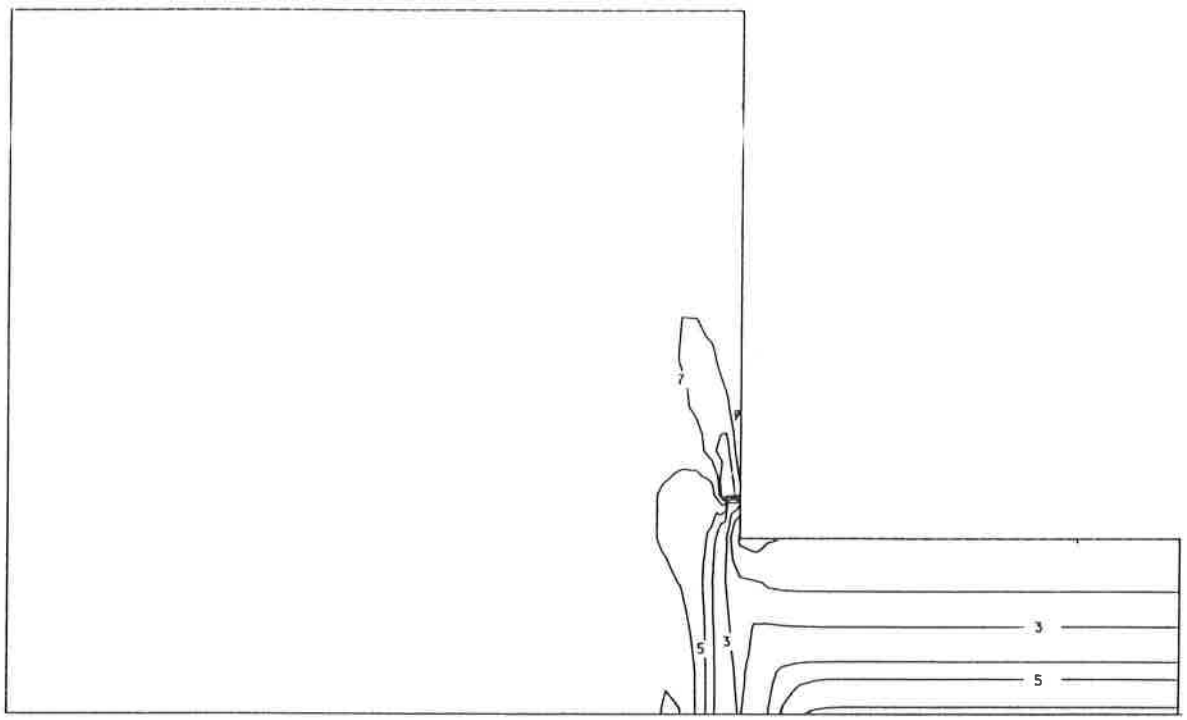

(b) PXY R=1, W=1

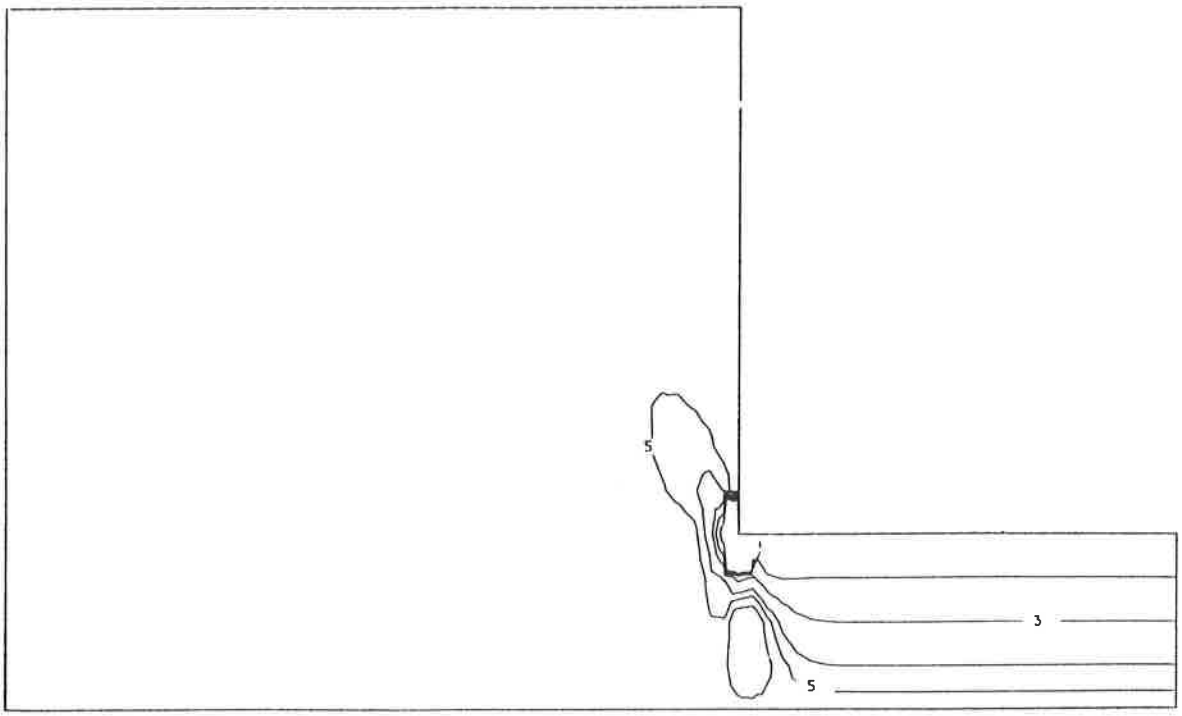

Fig. 6. (a) and (b)

(a) PXX-PYY R=1, W=1

CONTOUR KEY

1	1.00000
2	0.50000
3	0.25000
4	0.10000
5	0.05000
6	0.01000
7	-0.01000
8	-0.02000
9	-0.05000
10	-0.10000

(b) PXY R=1, W=1

CONTOUR KEY

1	1.00000
2	0.75000
3	0.50000
4	0.25000
5	0.10000
6	-0.10000
7	-0.50000
8	-1.00000
9	-2.00000
10	-5.00000

Fig. 6. (a) and (b)

(c) PXX-PYY R=1, W=10

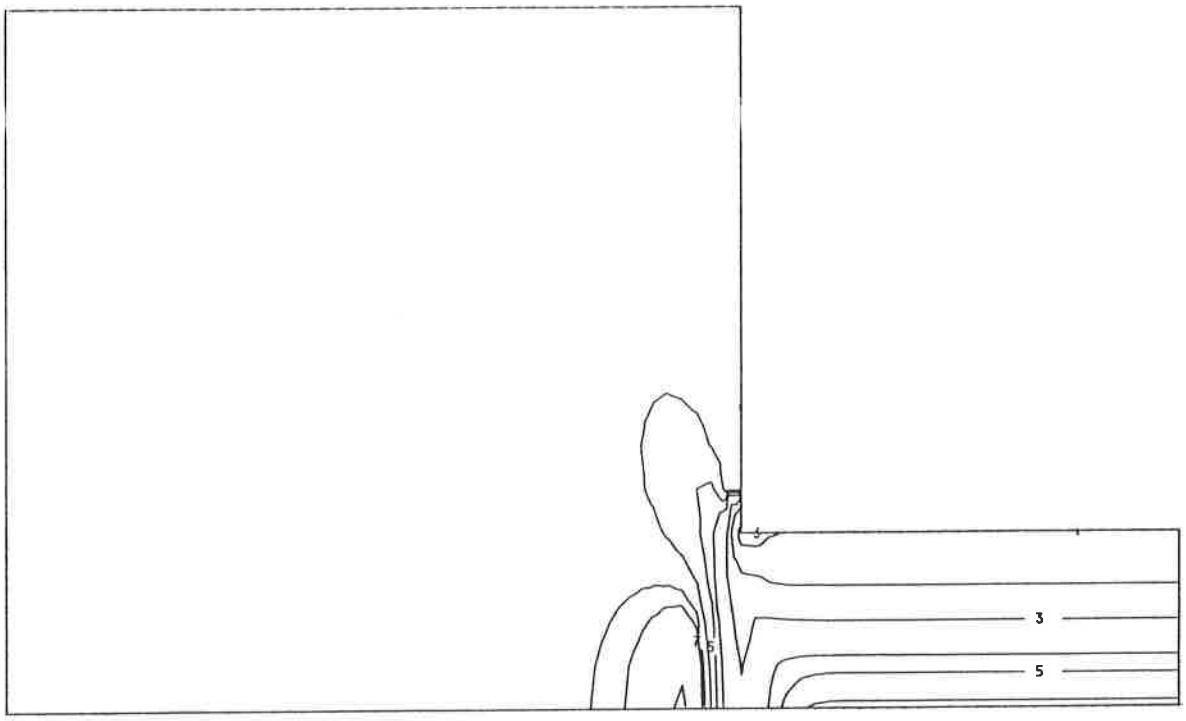

(d) PXY R=1, W=10

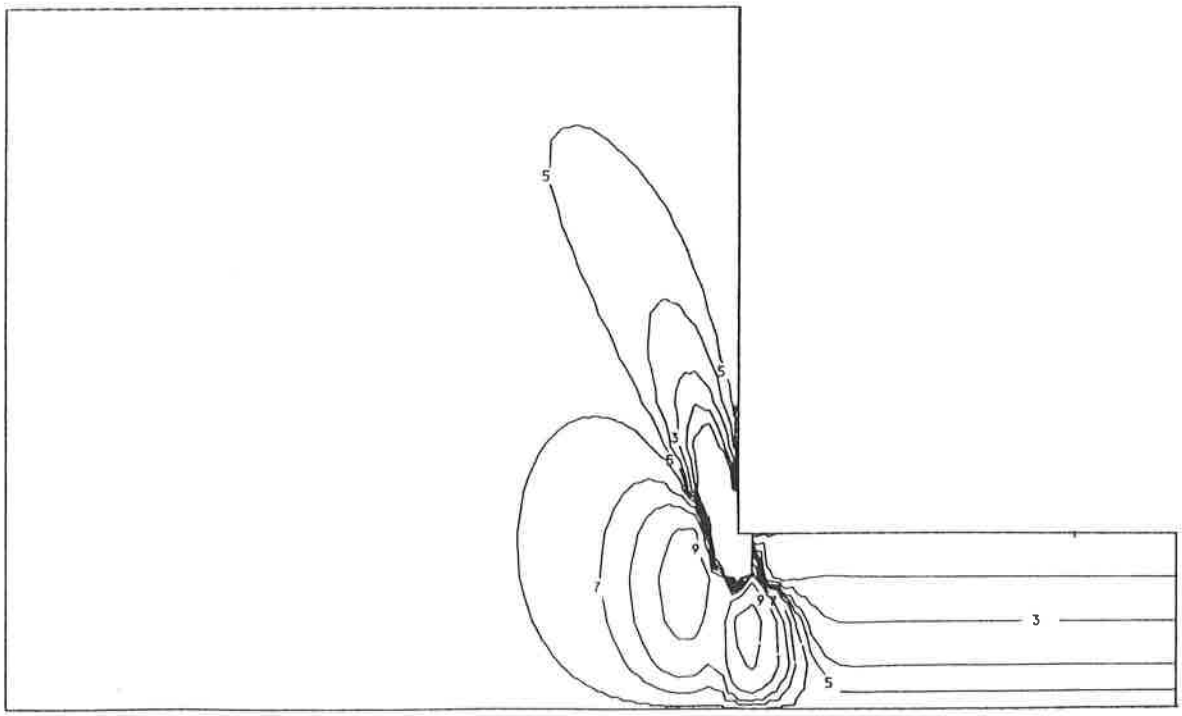

Fig. 6. (c) and (d)

(c) PXX-PYY R=1, W=10

CONTOUR KEY	
1	1.00000
2	0.50000
3	0.25000
4	0.10000
5	0.05000
6	0.01000
7	-0.01000
8	-0.02000
9	-0.05000
10	-0.10000

(d) PXY R=1, W=10

CONTOUR KEY	
1	1.00000
2	0.75000
3	0.50000
4	0.25000
5	0.10000
6	-0.10000
7	-0.50000
8	-1.00000
9	-2.00000
10	-5.00000

Fig. 6. (c) and (d)